Saudi Pharmaceutical Journal 28 (2020) 1155–1165

Contents lists available at ScienceDirect

Saudi Pharmaceutical Journal

journal homepage: www.sciencedirect.com

Original article

Galenia africana plant extract exhibits cytotoxicity in breast cancer cells by inducing multiple programmed cell death pathways

Luqmaan Mohamed [a,1], Suparna Chakraborty [a,1], K.N. ArulJothi [a,e], Lawrence Mabasa [c], Kenza Sayah [a], Leticia V. Costa-Lotufo [d], Anwar Jardine [b], Sharon Prince [a,d,*]

[a] Division of Cell Biology, Department of Human Biology, University of Cape Town, Cape Town 7925, South Africa
[b] Department of Chemistry, University of Cape Town, Cape Town 7925, South Africa
[c] Medical Research Council, Tygerberg 7505, South Africa
[d] Department of Pharmacology, Institute of Biomedical Science, University of São Paulo, São Paulo 05508-900, SP, Brazil
[e] Department of Genetic Engineering, Faculty of Engineering and Technology, SRM Institute of Science and Technology, Potheri, Chennai 603203, India

ARTICLE INFO

Article history:
Received 5 June 2020
Accepted 8 August 2020
Available online 14 August 2020

Keywords:
Galenia africana (Kraalbos)
Breast cancer
Cytotoxicity
Autophagy
Apoptosis
Necroptosis

ABSTRACT

Globally, breast cancer is the most common malignancy in women and the second most common cause of cancer-related death among women. There is therefore a need to identify more efficacious therapies for this neoplasm. *Galenia africana* (Kraalbos) is a perennial shrub found in Southern Africa and is used by the indigenous people to treat various ailments. There has therefore been much interest to establish the scientific basis for the medicinal properties of Kraalbos. This study aimed to investigate and characterise the anti-cancer activity of an ethanolic extract of Kraalbos leaves, KB2, against oestrogen receptor positive (MCF-7) and triple negative (MDA-MB-231) breast cancer cells. LC-MS/MS analyses identified the phytochemicals 7′-hydroxyflavanone, 5′,7′-dihydroxyflavanone, 2′,4′-dihydroxydihydrochalcone and 2′,4′-dihydroxychalcone in KB2. KB2 exhibited an IC_{50} of 114 μg/ml and 130.5 μg/ml in MCF-7 and MDA-MB-231 cells respectively, selectively inhibited their long-term survival and reduced their migration which correlated with a decrease in EMT markers. It induced oxidative stress (ROS), DNA damage (increased levels of γ-H2AX), and triggered cell cycle arrests in MCF-7 and MDA-MB-231 cells. Importantly, KB2 activated intrinsic (cleaved caspase 9) and extrinsic (cleaved caspase 8) apoptosis, necroptosis (p-RIP3 and the downstream target of the necrosome, pMLKL) and autophagy (LC3II). Co-treatment of the breast cancer cells with KB2 and the autophagy inhibitor bafilomycin A1 resulted in a significant increase in cell viability which suggests that KB2 induced autophagy is a cell death mechanism.

1. Introduction

Breast cancer is the most commonly diagnosed cancer and the principal cause of death from cancer among women globally (Bray et al., 2018). To reduce this burden, there is a pressing need to find effective therapies that exhibit minimal side effects. Accumulating evidence suggests that plant-derived compounds may prove extremely beneficial for the treatment of a broad spectrum of cancers. Indeed, several phytochemicals have entered clinical trials and are showing promise for the treatment of breast cancer. For example, the herbal preparation from Blue Citrus (NCT00702858) is currently in clinical trials for oestrogen receptor positive (ER+) post-menopausal breast cancer, and herbal extracts from *Scutellaria barbata* (NCT00028977) have passed phase II clinical trials for metastatic breast cancer. Furthemore, there is evidence that phytochemical derivatives can be used synergistically with other chemotherapeutic agents to treat cancer. Indeed, leaf extracts of *Strobilanthes crispus* in combination with tamoxifen induced apoptosis in ER+ and triple negative (TN) breast cancer cells (Yaacob et al., 2014).

Galenia africana is a perennial shrub also known as Kraalbos or Geelbos. It is indigenous to Southern Africa and is found mainly in the Namaqualand and Karoo regions. The indigenous Khoisan people and the inhabitants of the Namaqua region have long been

* Corresponding author at: Room 6.05.1, Level 6, Anatomy Building, Anzio Road, Observatory, Cape Town 7925, South Africa.
E-mail address: sharon.prince@uct.ac.za (S. Prince).
[1] Authors contributed equally.
Peer review under responsibility of King Saud University.

Production and hosting by Elsevier

https://doi.org/10.1016/j.jsps.2020.08.004
1319-0164/

aware of the medicinal properties of Kraalbos. It has been traditionally used to treat a variety of ailments such as skin rashes, dandruff and dry scalp, coughs and wounds (Van Wyk et al., 2008). It is also a known analgesic used to treat toothache and has been used to treat respiratory conditions such as asthma and tuberculosis (Van De Beer and Wyk, 2011; Mativandlela et al., 2009, 2008). This versatility in the traditional use of Kraalbos as a medicinal agent and its panacea like status among the indigenous people have been the impetus for the scientific investigation of its medicinal properties. Several studies have demonstrated the activity of Kraalbos extracts against a broad variety of biological pathogens. Elbagory et al. (2017) reported that gold nanoparticles encasing an aqueous Kraalbos extract showed anti-microbial properties against *Pseudomonas aeruginosa*. Extracts of Kraalbos also exhibited anti-mycobacterial effects against both *Mycobacterium smegmatis* and *Mycobaterium tuberculosis* (Mativandlela et al., 2009, 2008). Similarly, ethanolic extracts derived from the aerial parts of the Kraalbos plant have been reported to display anti-fungal activity (Vries et al., 2005). Thus, there is a growing pool of scientific literature that provides credibility to the anecdotal claims of Kraalbos as a medicinal agent.

While there is some evidence that Kraalbos extracts may also have anti-cancer activity, its application in the treatment of cancer is poorly understood. The aim of this study was to determine the anti-cancer activity of an ethanolic Kraalbos extract (KB2) against ER+ (MCF-7) and TN (MDA-MB-231) breast cancer cells. To this end, we investigated the impact of KB2 on short- and long-term cytotoxicity, breast cancer cell selectivity, and migration. This study also aimed to elucidate the mechanism by which KB2 exerts its cytotoxicity in breast cancer cells by investigating its effects on ROS production, DNA damage, the cell cycle, and programmed cell death pathways such as apoptosis, necroptosis and autophagy.

2. Materials and methods

2.1. Cell lines and culture

ER+ breast adenocarcinoma MCF-7 cells were cultured in RPMI 1640 medium and the non-malignant fibroblast, FG0, and TN breast adenocarcinoma MDA-MB-231 cells were maintained in DMEM. The non-malignant breast epithelial cells (MCF-12A) were maintained in a 1:1 mixture of DMEM and Ham's F12 medium supplemented with 100 ng/ml cholera toxin and 20 ng/ml epidermal growth factor (Sigma-Aldrich, Missouri, USA), 500 ng/ml hydrocortisone (Calbiochem, California, USA), and 10 μg/ml insulin (Novo Nordisk, Bagsværd, Denmark). All media (Gibco®, Life Technologies New York) were supplemented with 10% fetal bovine serum (Gibco®, Life Technologies, New York), 100 U/ml penicillin and 100 μg/ml streptomycin (Sigma-Aldrich, Missouri, USA).

2.2. Harvesting and extraction

The Kraalbos plant was harvested from the Kommagas region in the Northern Cape, South Africa. The leaves, shoots and twigs were sundried and milled using a hammer mill. The raw material was then subjected to extraction using a 1:8 of 60% ethanol as a solvent at 60–65 °C for 4 h. The extract was then filtered and subjected to vacuum drying (80–90% vacuum) at 70–75 °C to yield the final KB2 extract. KB2 was dissolved in DMSO to obtain a 20 mg/ml stock and the stock was serially diluted using the appropriate medium to prepare the working solutions.

2.3. LC-MS/MS analysis of KB2

The extract was analyzed by liquid chromatography and electrospray ionization mass spectrometry according to previously described methods (Keskes et al., 2017). For chromatographic separations, an Agilent 1290 HPLC system (Agilent Technologies, USA) equipped with infinity binary pump was used. The compounds were separated at 40 °C on a Phenomenex Kinetex C18 column (100 mm × 2.1 mm × 1.7 μm; Agilent Technologies, USA) with two mobile phases containing H_2O with 0.1% formic acid (A) and acetonitrile with 0.1% formic acid (B) at a flow rate of 0.35 ml/min for 9 min. MS detection was performed in a 4500 Qtrap mass spectrometer (AB Sciex, USA) equipped with electrospray ionization source (ESI) and a triple quadrupole-ion trap mass analyzer. The injected amount of ethanolic extract of KB2 was 5 μl on the 4500 Q-Trap. The ESI worked with the negative ion mode at the following conditions: capillary temperature 450 °C, curtain gas at 35 psi and nebulizer gas at 40 psi, negative ionization mode source at −4500 V and nitrogen was used as curtain and collision gas. The analytes were identified by comparing retention time and m/z values obtained by MS/MS from corresponding standards. The MRM transitions used to monitor the analytes, 7′-hydroxyflavanone, 5′,7′-dihydroxyflavanone (pinocembrin), 2′,4′-dihydroxychalcone and 2′,4′-dihydroxydihydrochalcone were (239 → 91), (255 → 107), (239 → 197) and (241 → 109) respectively. The certified analytical standards pinocembrin (Sigma-Aldrich, P5239) and 2,'4′-dihydroxychalcone (Indofine, D504) were used at a concentration range from 0.05 to 25 ppm. Doped standards [1000 ppm of the pinocembrin and 2,'4′-dihydroxychalcone were mixed to prepare a 500 ppm working stock] were included. Certified reference standards were used to setup a multi-point calibration curve for quantification of the actives. The area under the curve was used for quantification.

2.4. Cell-Titer Glo® assay

Cells were seeded in 96 well plates and treated with vehicle or KB2 for 48 h. The Cell-Titer Glo® Luminescent cell viability assay (Promega, Wisconsin, USA) was performed following the manufacturer's instructions. Luminescence was measured using a fluorometer (GloMax® Explorer Promega, Wisconsin, USA). Three independent experiments were performed to determine the half maximal inhibitory concentration values (IC_{50}) of KB2 using GraphPad Prism version 6.0 (California, USA). The selectivity index (SI) of KB2 was determined by dividing its IC_{50} in a non-malignant cell line by its IC_{50} in a breast cancer cell line.

2.5. Clonogenic assays

Cells were seeded at 2.5–3.0 × 10^5 cells per 6 cm dish and treated with vehicle or KB2 for 24 h. Cells were then trypsinized, washed with PBS and re-plated at low densities (800–2000 cells per 35 mm dishes) and allowed to form colonies for 7–21 days depending on the cell line. The clonogenic assays were performed as described by Bleloch et al. (2019).

2.6. In vitro cell migration assay

Cells were seeded in 12 well plates and allowed to reach 100% confluency and a scratch motility assay was performed as described by Bleloch et al. (2019). On the day that the scratch was made, the cells were treated with vehicle or KB2 and the wound was monitored and photographed using the Evos® XL Core microscope (Thermo Fisher Scientific, Massachusetts, USA) at 3 h intervals for up to 24 h. The areas of the wounds were measured using the ImageJ software. The area of the wound at each time

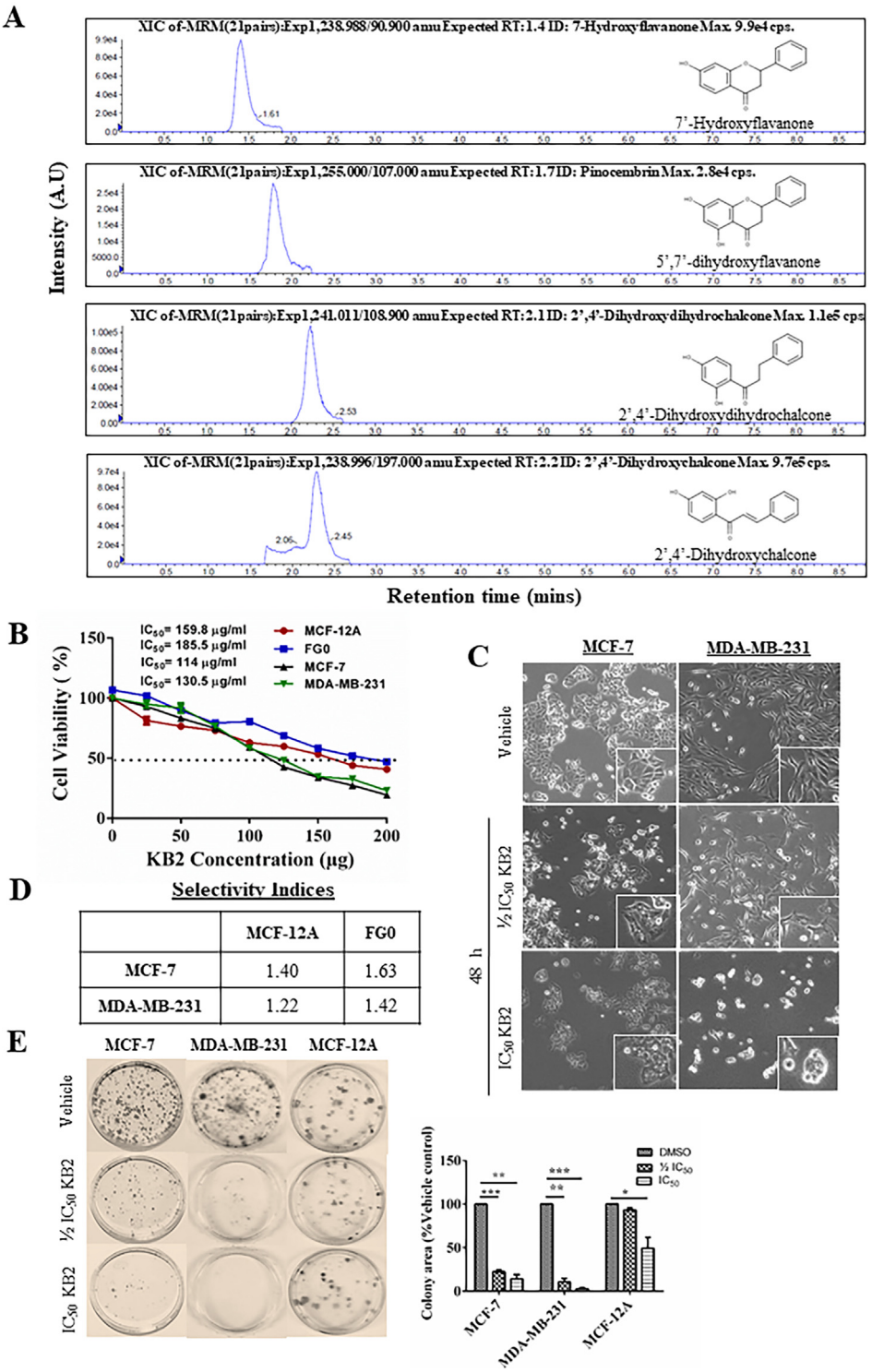

	MCF-12A	FG0
MCF-7	1.40	1.63
MDA-MB-231	1.22	1.42

Fig. 1. Phytochemical composition and short- and long-term cytotoxicity of KB2. (A) MS/MS data from the LC fractions eluted between 0 min and 9 min running time. The compounds and their corresponding structures are shown alongside the chromatogram. The MRM transitions used to monitor the analytes, 7′-hydroxy flavanone, 5′,7′-dihydroxyflavanone (pinocembrin), 2′,4′-dihydroxychalcone and 2′,4′-dihydroxydihydrochalcone were (239 → 91), (255 → 107), (239 → 197) and (241 → 109) respectively. (B) Short-term cytotoxicity in cells treated with a range of KB2 concentrations (0–200 µg/ml) for 48 h. (C) Representative images of MCF-7 (left panel) and MDA-MB-231 (right panel) cells treated as indicated and captured using light microscopy (200×). (D) Selectivity indices of KB2. (E) Representative images and quantification of clonogenic assays. Colonies were stained with crystal violet, photographed and the areas of the colonies measured using the ColonyArea plugin for ImageJ. The graph represents the mean colony area ± SEM of each treatment as a percentage of the vehicle control for experiments done in triplicate. Data was analysed using GraphPad Prism 6.0 and a parametric unpaired *t*-test was performed where $^{*}p \leq 0.05$, $^{**}p \leq 0.01$ and $^{***}p \leq 0.001$.

point was measured and subtracted from the area at time zero to yield the migrated area.

2.7. Flow cytometry analysis

The cells were treated with vehicle or KB2 for 48 h and processed as previously described (Bleloch et al., 2019). The cell cycle profiling was done using the BD FACS Calibur flow cytometer (Becton Dickinson, New Jersey, USA) with a 488 nm Coherent laser (Santa Clara, California, USA). The Cell quest Pro version 5.2.1 software was used for data acquisition.

2.8. Oxidative stress detection assays

The levels of H_2O_2 (ROS) and glutathione (antioxidant) were measured using the ROS-Glo™ H_2O_2 and GSH-Glo™ Glutathione assay kits (Promega, Wisconsin, USA) respectively following the manufacturer's instructions and the results were read using the GloMax® Explorer machine (Promega, Wisconsin, USA).

2.9. Western blotting

The cells were treated with vehicle or KB2 for 24 h and 48 h. The cells were lysed in whole-cell lysis buffer and western blotting was

Table 1
Phytochemical composition of the ethanolic extract KB2 obtained from *Galenia africana*.

Compound	Chemical formula	Retention time (t_R) (min)	*m/z* calculated	MW	%
7′-hydroxyflavanone	$C_{15}H_{12}O_3$	1.4	238.9	240.25	1.9
5′,7′-dihydroxyflavanone (pinocembrin)	$C_{15}H_{12}O_4$	1.7	255.0	256.25	7.4
2′,4′-dihydroxydihydrochalcone	$C_{15}H_{14}O_3$	2.1	241.0	242.27	1.8
2′,4′-dihydroxychalcone	$C_{15}H_{12}O_3$	2.2	238.9	240.25	7.4

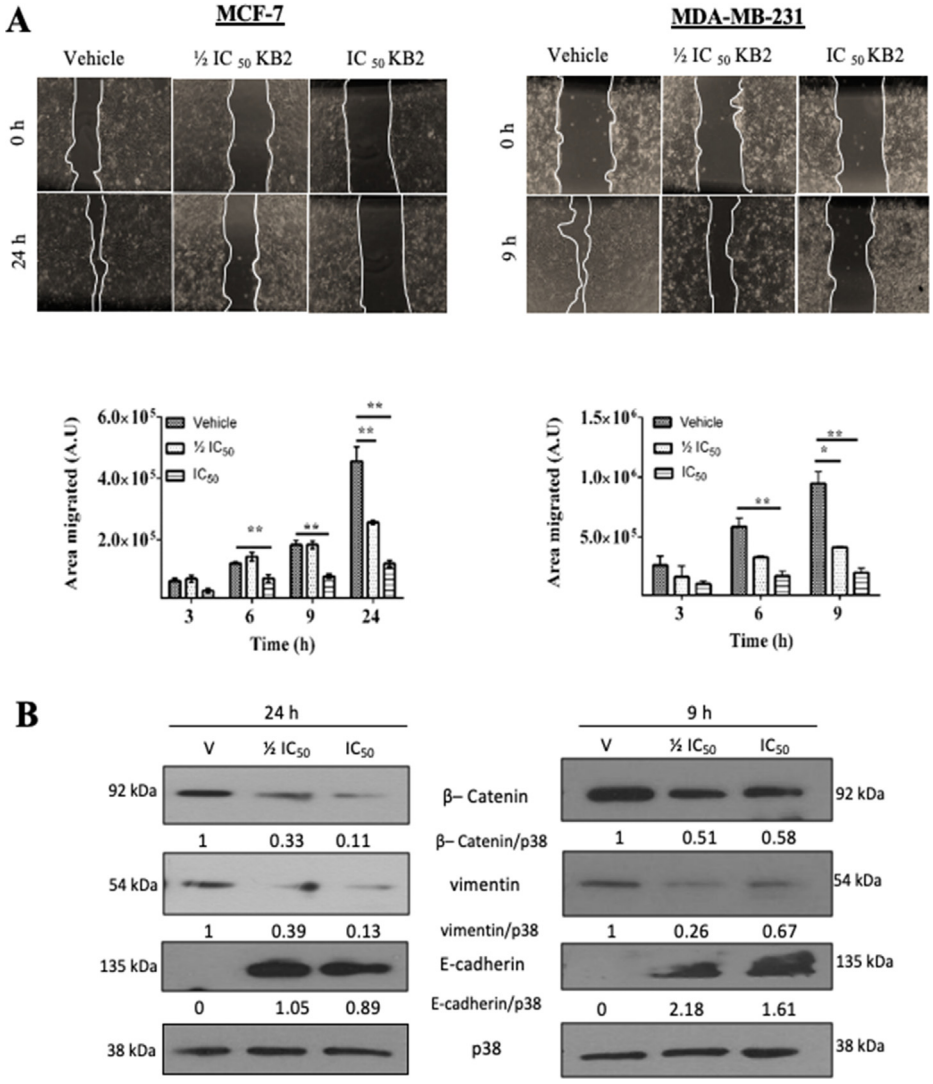

Fig. 2. KB2 inhibits breast cancer cell migration. (A) Representative images and quantification of scratch motility assay of cells treated as indicated taken at the specified time points. Graphs represent mean area migrated ± SEM pooled from three independent repeats. Data was analysed using GraphPad Prism 6.0 and a parametric unpaired *t*-test was performed where $^*p < 0.05$, $^{**}p < 0.01$, $^{***}p < 0.001$. (B) Western blot analyses of protein harvested from MCF-7 (left panel) and MDA-MB-231 (right panel) cells treated as indicated and incubated with antibodies to EMT markers: E-cadherin, β-catenin and vimentin.

carried out as previously described (Bleloch et al., 2019). The primary antibodies used in this study were, rabbit polyclonal antibodies to phospho-histone H2A.X (Ser139) (#2577), cleaved caspase-3 (Asp175) (#9661), PARP (#9542), caspase-9 (#9502), LC3II (#2775), rabbit monoclonal antibody to β-Catenin (D10A8) (#8480), cleaved caspase-7 (Asp198) (D6H1) (#8438), mouse monoclonal antibodies to E-cadherin (4A2) (#14472), vimentin (R28) (#3932), Cyclin B1 (V152) (#4135), Caspase-8 (1C12) (#9746) from Cell Signaling Technology (Massachusetts, USA); mouse monoclonal antibody to p53 (DO-1) (sc-126), rabbit polyclonal antibodies to p21 (C-19) (sc-397), Cyclin A (H-432) (sc-751) from Santa Cruz Biotechnology (Texas, USA); rabbit polyclonal antibody to p38 MAP kinase (M0800) from Sigma Aldrich. After primary antibody incubation, membranes were incubated with goat anti-rabbit or goat anti-mouse HRP-conjugated secondary antibodies (Bio-Rad Laboratories, California, USA). p38 was used as a loading

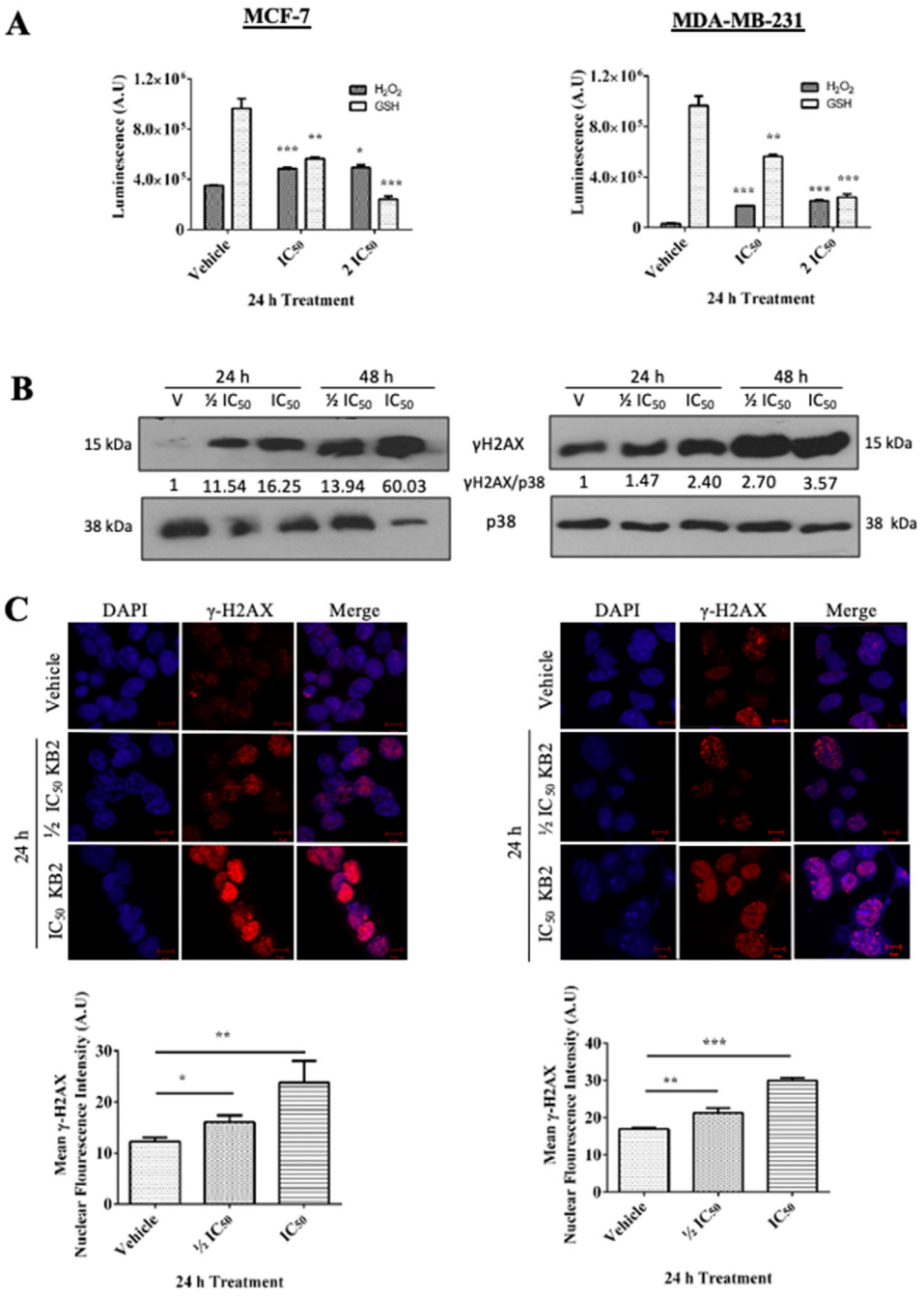

Fig. 3. KB2 induces DNA damage in breast cancer cells. (A) H_2O_2 and GSH levels were measured using ROS-Glo™ H_2O_2 and GSH-Glo™ Glutathione assay kits from the cells treated as indicated. Graph represents mean levels of H_2O_2 and GSH ± SEM pooled from two independent repeats. Data was analysed using GraphPad Prism 6.0 and a parametric unpaired *t*-test was performed relative to vehicle treated cells where $^{*}p < 0.05$, $^{**}p < 0.01$, $^{***}p < 0.001$. (B) Western blot analyses of protein harvested from MCF-7 (left panel) and MDA-MB-231 (right panel) cells treated as indicated and incubated with antibodies to γ-H2AX. (C) Representative images of MCF-7 (left panel) and MDA-MB-231 (right panel) cells treated as indicated and processed by immunocytochemistry for γ-H2AX levels (Cy3 channel). Quantification is representative of the intensity of the γ-H2AX signal from 20 fields of view from three independent repeats. Data was analysed using GraphPad Prism 6.0 and a parametric unpaired *t*-test was performed where $^{*}p < 0.05$, $^{**}p < 0.01$, $^{***}p < 0.001$.

control. Densitometry readings were obtained using ImageJ and protein expression levels are represented as a ratio of protein of interest/p38 normalized to the vehicle control sample.

2.10. Immunocytochemistry

Cells were treated with vehicle or KB2 for 24 h or 48 h and immunocytochemistry and analyses thereof carried out as previously described (Bleloch et al., 2019). Briefly, before treatment, cells were seeded on glass coverslips in 35 mm dishes. After treatment cells were fixed with ice cold methanol, then permeabilised and blocked. Slides were incubated with antibodies against phospho-histone H2A.X (#2577) or LC3B (#2775) (Cell Signaling Technology) in blocking buffer overnight at 4 °C. The following day, slides were incubated with donkey anti-rabbit Cy3-conjugated secondary antibodies (Jackson ImmunoResearch Laboratories Inc., Pennsylvania, USA) and the nuclei were stained with Hoechst. Images were obtained on a Carl Zeiss LSM 880 with Fast Airyscan module confocal microscope and analysis was carried out using he Zen software.

2.11. Statistical analysis

All experiments were repeated three times with at least three technical repeats per experiment, unless stated otherwise. Statistical analyses were carried out on data pooled from all biological repeats using Graphpad prism version 6.0 and values are presented as mean ± standard deviation. Significance was determined using a student *t*-test, $p < 0.05$ indicated statistical significance.

3. Results and discussion

3.1. Phytochemical composition of KB2

To identify the active compounds present in the KB2 ethanolic extract of *Galenia Africana* we performed LC-MS/MS analysis. The results shown in Fig. 1A and Table 1 revealed that the extract consisted of a mixture of 7-hydroxyflavanone (1.9%), 5,7-dihydroxyflavanone (pinocembrin) (7.4%), 2′,4′-dihydroxydihydro chalcone (1.8%) and 2′,4′-dihydroxychalcone (7.4%) which are minor flavonoids found in small amounts only in plants (Clifford and Toma, 2000). The composition of KB2 is interesting in light of reports from epidemiological studies and clinical trials that flavanoids have major roles in cancer prevention and chemotherapy. Specifically, while flavanones have shown anti- oral and -breast cancer activity, chalcones have shown anti-cancer activity in oral cancer and leukemia (Chahar et al., 2011). In this regard, it is worth noting that pinocembrin was also previously identified in Kraalbos extracts (Mativandlela et al., 2009; Ng'uni, 2017; Ticha et al., 2015; Vries et al., 2005) and that pinocembrin has been shown to exhibit anti-cancer effects against a variety of cancers including colon cancer, prostate cancer and leukemia (Chen et al., 2013; Kumar et al., 2007; Rasul et al., 2013). Given the known anti-cancer activity of flavonoids it is tempting to speculate that they are responsible

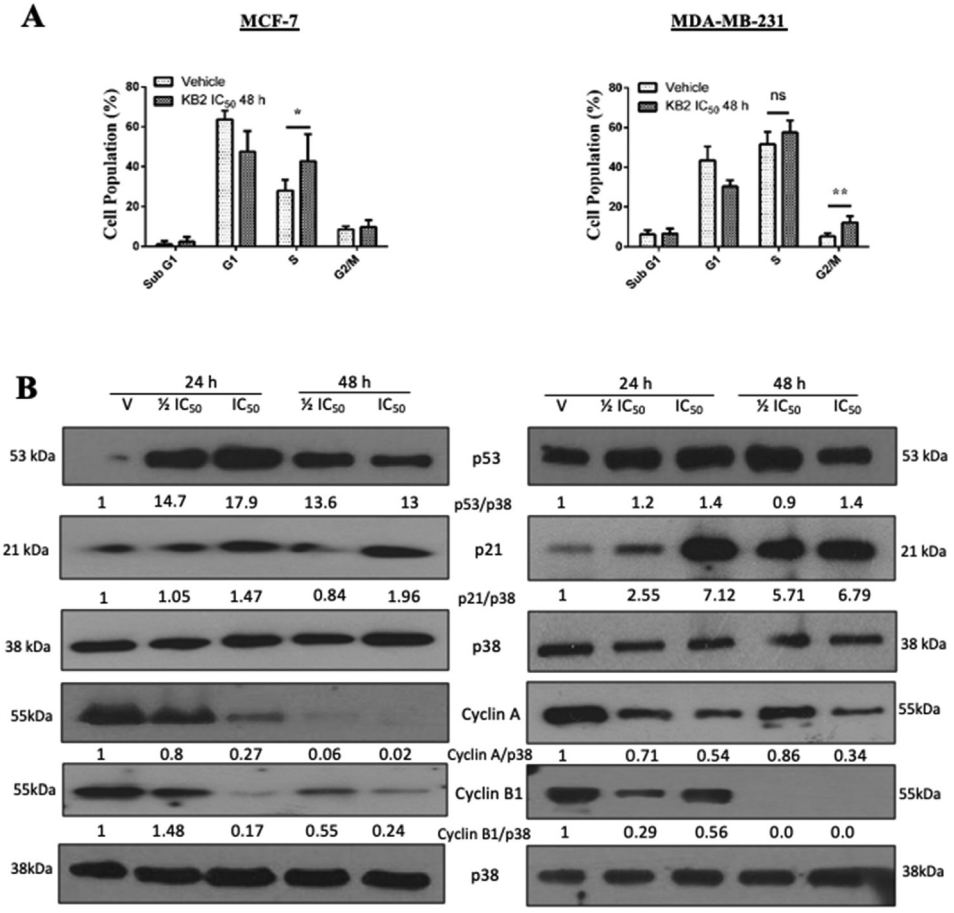

Fig. 4. KB2 induces cell cycle arrests in breast cancer cells. (A) Flow cytometry analysis of cells treated as indicated, the bar graphs show the percentage of the cells at each phase of the cell cycle pooled from three independent repeats. Data was analysed using GraphPad Prism 6.0 and a parametric unpaired *t*-test was performed where *p < 0.05, **p < 0.01, ***p < 0.001. (B) Western blot analyses of protein harvested from MCF-7 (left panel) and MDA-MB-231 (right panel) cells treated as indicated and incubated with antibodies to the cell cycle regulators: p53, p21, Cyclin A and B1.

for the anti-cancer activity exhibited by KB2 either solely or that they work synergistically with other, as yet to be identified compounds, present in the KB2 extract.

3.2. KB2 exerts short-term and long-term cytotoxicity in breast cancer cells

To determine the short-term cytotoxicity of KB2 in breast cancer cells, the Cell-Titer® Glo assay was used. The results showed that KB2 exhibited an IC_{50} of 114.0 μg/ml and 130.5 μg/ml in ER + MCF-7 and TN MDA-MB-231 cells respectively (Fig. 1B). It is worth noting that, Ng'uni (2017) obtained an IC_{50} of 1250 μg/ml for a Kraalbos extract in MCF-7 cells which is 11 times more than what we obtained for KB2. It is possible that the difference in IC_{50} values is due to the preparation of KB2 used in our study having been through more processing steps and therefore being more pure. Light microscopy confirmed that KB2 reduced the viability of the breast cancer cells in a dose dependent manner (Fig. 1C). To determine the selectivity of KB2 for breast cancer cells, we next determined its IC_{50} in non-malignant fibroblasts (FG0) and breast epithelial cells (MCF-12A) and values of 185.5 μg/ml and 159.8 μg/ml respectively were obtained. These results indicated that ER+ and TN breast cancer cells were slightly more sensitive to KB2 than non-malignant cells with approximate selectivity indices (SI) ranging from 1.22 to 1.63 (Fig. 1D).

The clonogenic assay is considered a powerful tool to predict the sensitivity or resistance that cancer patients may have to an anti-cancer drug (Fiebig et al., 2004). Briefly, the assay involves testing the colony forming ability of cancer cells after their long-term exposure to a potential anti-cancer drug. We therefore next investigated the effect of KB2 on MCF-7 and MDA-MB-231 breast cancer cells in clonogenic assays and we included the MCF-12A non-malignant breast epithelial cells as a control. The results showed that ½ IC_{50} and IC_{50} KB2 significantly inhibited the survival and proliferation of MCF-7 and MDA-MB-231 breast cancer cells (Fig. 1E). Importantly, whereas ½ IC_{50} KB2 had no significant effect on the survival of the non-malignant MCF-12A cells, it inhibited survival of 86% and 96% of the MCF-7 and MDA-MB-231 breast cancer cells respectively. These results are important because they reveal that while, in the short-term cell viability assays, KB2 had SI

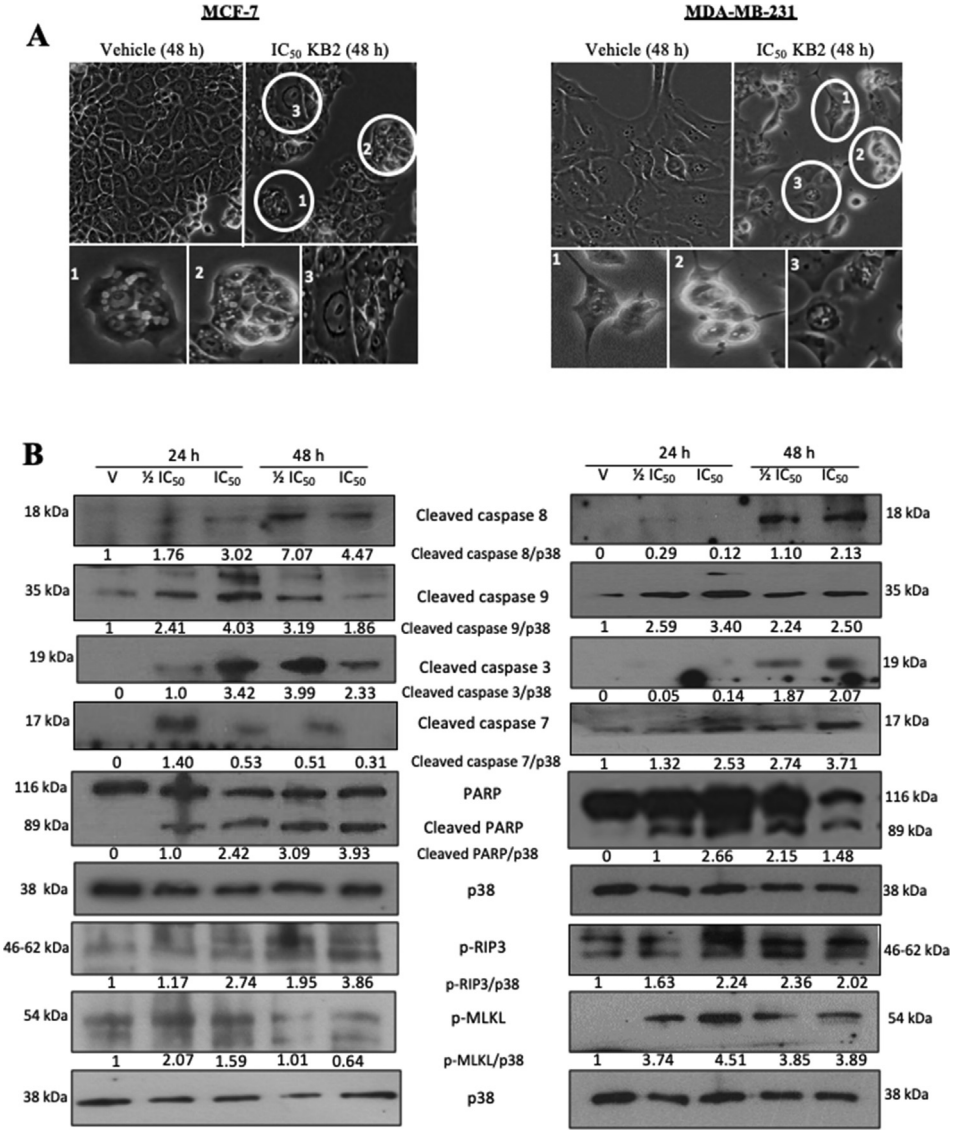

Fig. 5. KB2 induces apoptosis and necroptosis in breast cancer cells. (A) Representative light microcopy images (200×) of cells treated as indicated. Numbered circles correspond to magnified images below which highlight (1) cell shrinkage, (2) membrane blebbing and (3) chromatin condensation. (B) Western blot analyses of protein harvested from MCF-7 (left panel) and MDA-MB-231 (right panel) cells treated as indicated and incubated with antibodies to apoptotic markers: Cleaved caspases 9, 8, 7, 3 and cleaved PARP and necroptotic markers: p-RIP3 and p-MLKL.

values below the recommended value of 2 (Koch et al., 2005), it exhibited greater selectivity for the breast cancer cells in the long-term survival assays. Furthermore, the sensitivity displayed by the MDA-MB-231 cells to KB2 is promising because it represents a TN breast cancer which are notoriously recalcitrant to current therapies.

3.3. KB2 inhibits breast cancer cell migration

The ability of breast cancer cells to migrate from the primary site to form metastatic tumours in distant organs is the main cause of morbidity. We therefore investigated the effect of KB2 on the ability of MCF-7 and MDA-MB-231 cells to migrate using a scratch

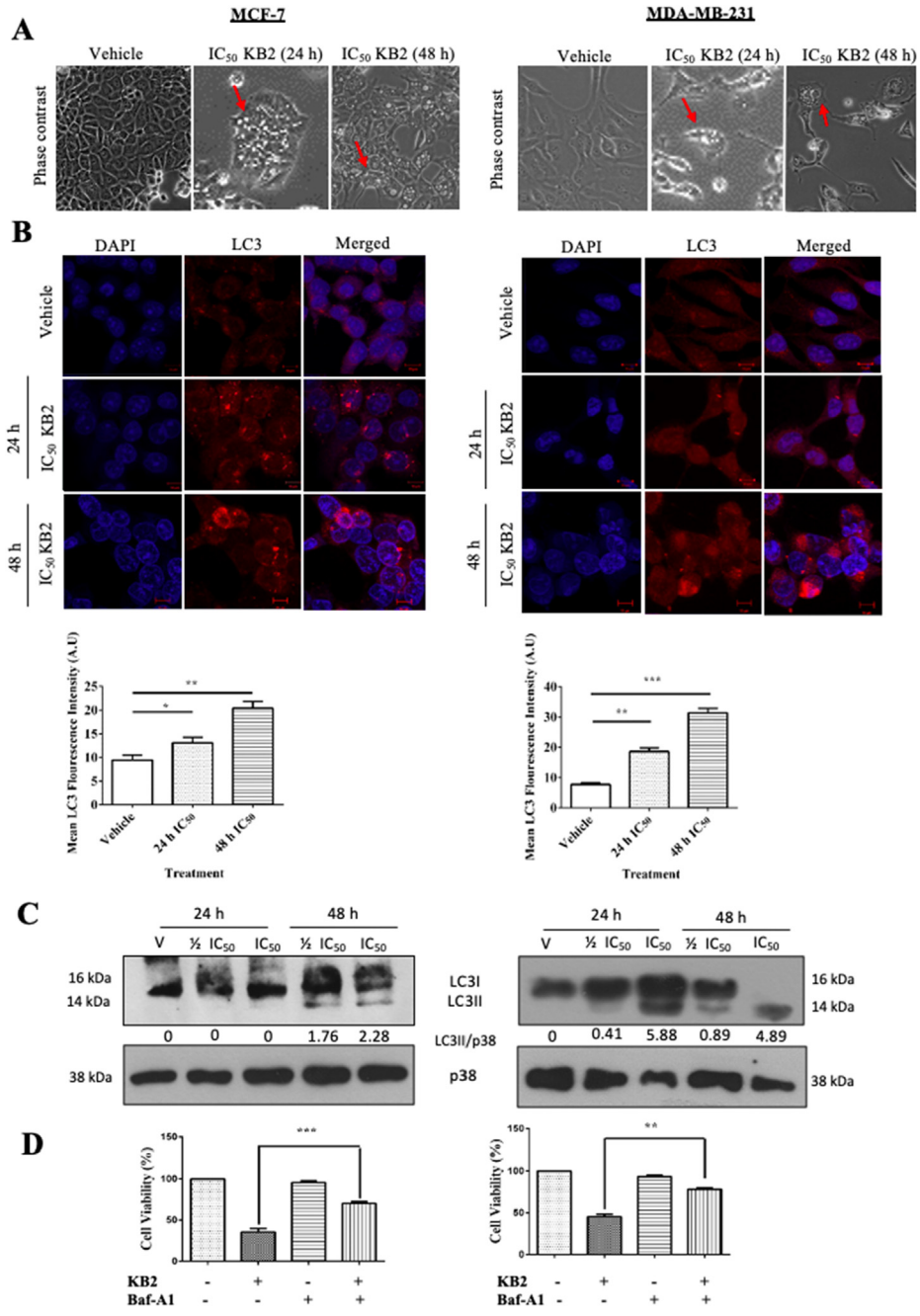

Fig. 6. KB2 induces autophagy in breast cancer cells. (A) Representative light microcopy images (200×) from cells treated as indicated, red arrows showing vacuolar structures. (B) Representative confocal immunofluorescence images (630×; scale bar is 20 μm) from three independent repeats of MCF-7 (left panel) and MDA-MB-231 (right panel) cells treated as indicated and incubated with LC3 primary antibody, fluorophore conjugated Cy3 secondary antibody and nuclei were stained with DAPI. Bar graphs show quantification of LC3 staining representative of the intensity of the LC3 signal from 20 fields of view from three independent repeats. Data were analysed using GraphPad Prism 6.0 and a parametric unpaired *t*-test was performed where *p < 0.05, **p < 0.01, ***p < 0.001. (C) Western blot analyses of protein harvested from MCF-7 (left panel) and MDA-MB-231 (right panel) cells treated as indicated and incubated with antibodies to LC3. (D) MTT assays showing cell viability of MCF-7 (left panel) and MDA-MB-231 (right panel) cells treated with KB2 or vehicle for 48 h followed by 2 h of treatment with 200 nM bafilomycin A1. Bar graphs show mean cell viability as a percentage of vehicle control ± SEM determined from three independent experiments performed in quadruplicate. Data was analysed using Graph Pad Prism 6.0 and a parametric unpaired *t*-test was performed where *p < 0.05, **p < 0.01, ***p < 0.001.

motility assay. The results showed that KB2 significantly reduced the migratory ability of both breast cancer cell lines in a dose dependent manner (Fig. 2A). Epithelial to mesenchymal transition (EMT) describes a process where epithelial cells lose their adhesive properties and acquire a fibroblast-like morphology and increased motility (Dongre and Weinberg, 2019). It confers upon cancer cells increased metastatic and invasive properties and greater resistance to chemotherapy and immunotherapy (Qian et al., 2017). Thus, targeting the EMT process is a potentially important approach for suppressing breast cancer cell metastasis. We therefore analysed the effect of KB2 on EMT markers using western blotting with protein harvested when the scratch in vehicle treated cells reached >95% closure. Due to their metastatic ability the MDA-MB-231 cells were able to achieve this more rapidly (9 h) than the MCF-7 cells (24 h). The results show that the KB2-inhibition of breast cancer cell migration correlated with the downregulation of the mesenchymal markers, β-Catenin and vimentin, and the induction of the epithelial marker, E-cadherin (Fig. 2B). These results are consistent with reports that the flavonoid Luteolin inhibited invasion of MDA-MB-231 cells by upregulating E-cadherin and downregulating the mesenchymal markers vimentin, N-cadherin, SNAIL and SLUG (Eichsteininger et al., 2019). Together, the data showed that KB2 exhibited several anti-breast cancer properties.

3.4. KB2 induces oxidative stress and DNA damage in breast cancer cells

One of the mechanisms by which phytochemicals kill cancer cells is by inducing an oxidative stress through the generation of ROS which leads to a decrease in antioxidants and damage to DNA, RNA, protein and lipid molecules resulting in apoptosis (Vallejo et al., 2017). Therefore, to begin to investigate the mechanism(s) by which KB2 exerted cytotoxicity in breast cancer cells, we measured the effect of KB2 on levels of the free radical, H_2O_2, and the antioxidant, glutathione. Our results showed that KB2 treatment led to an increase in H_2O_2 levels and a decrease in glutathione levels (Fig. 3A). This suggested that KB2 induced ROS production while reducing antioxidants which is consistent with what has been observed for other natural products and extracts (Chen et al., 2009; Tiloke et al., 2013).

We next investigated whether KB2 induced double strand DNA breaks in MCF-7 and MDA-MB-231 breast cancer cells by performing western blotting and immunofluorescence with an antibody to γ-H2AX. Our results showed that KB2 treatment led to a dose dependent increase in γ-H2AX levels (Fig. 3B) and nuclei puncta (Fig. 3C). Together these results indicate that KB2 induces both ROS and DNA damage in breast cancer cells. It is likely that the induced DNA damage is a direct consequence of ROS production as other natural products, such as the polyphenol curcumin, have been shown to cause ROS induced DNA damage (Navaneethakrishnan et al., 2019). Quercitin, another polyphenolic natural product, has been shown to induce DNA damage by intercalating with DNA as well as interfering with DNA topoisomerase II (Srivastava et al., 2016; Zhang et al., 2015). Thus the possibility that KB2 induces DNA damage by mechanisms independent of ROS cannot be ruled out.

3.5. KB2 inhibits breast cancer cell cycle progression

In response to DNA double strand breaks, cells activate cell cycle checkpoints to allow for the repair of the damaged DNA but if the damage is too great they undergo programmed cell death (Shaltiel et al., 2015). We therefore analyzed the effect of KB2 on the cell cycle profile of the breast cancer cells using flow cytometry. The results revealed that KB2 treatment resulted in an accumulation of MCF-7 cells in the S-phase and an accumulation of MDA-MB-231 cells in G2/M (Fig. 4A). In response to genotoxic (DSBs) and oxidative (ROS) stress the tumor suppressor p53 and the cyclin dependent kinase (CDK) inhibitor, $p21^{WAF1/Cip1}$ (hereafter referred to as p21), are important mediators of cell cycle arrest and cell death. p21, which can be induced in a p53-dependent and p53-independent manner, promotes cell cycle arrests by binding to and inhibiting the activity of cyclin-CDK1, -CDK2, and -CDK4/6 complexes (Johnson and Walker, 1999). Western blot analyses revealed that upon KB2 treatment MCF-7 cells upregulated p53 levels but p53 levels remained largely unchanged in MDA-MB-231 cells which is probably due them expressing a mutated form of p53 (Fig. 4B). Importantly, KB2 treatment of both breast cancer cell lines resulted in an upregulation of p21 levels and a decrease in the levels of Cyclins A and B1 (Fig. 4B). Together, the results suggested that KB2 activated p21 in a p53-dependent and -independent manner to block MCF-7 and MDA-MB-231 cell cycle progression by downregulating Cyclins A and B1. This series of events is consistent with results from other studies that have investigated the effects of oxidative stress on cancer cells (Russo et al., 1995). Furthermore, pinocembrin, was also reported to induce an S-phase cell cycle arrest in LNCaP prostate cancer cells (Chen et al., 2013) and a pinocembrin derivative (5-hydroxy-4-oxo-2-phenylchroman-7-yl 3,4,5-trimethoxybenzoate) exhibited anti proliferative activity in MDA-MB-231 cells (Cappello et al., 2019).

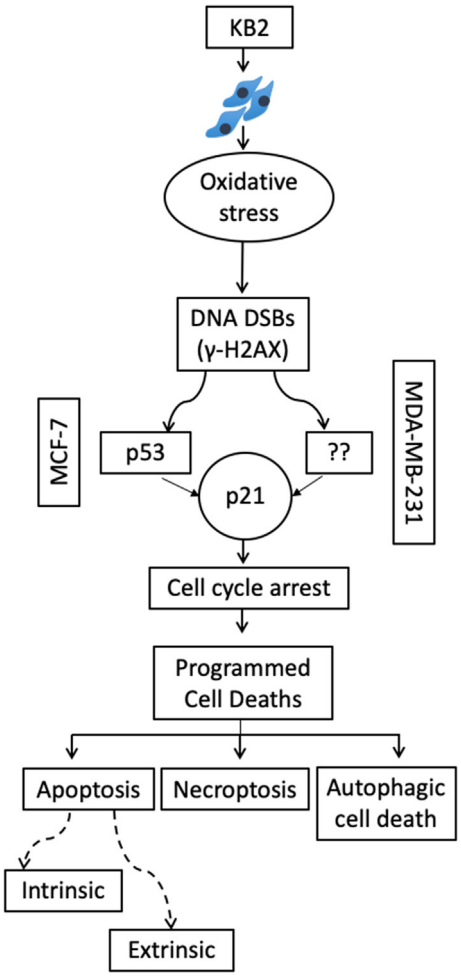

Fig. 7. Proposed model for mechanism of cytotoxic activity of KB2 in breast cancer cells. KB2 induces oxidative stress which induces DNA double strand breaks (DSBs) leading to activation of p21 in a p53 dependent and independent manner. This results in cell cycle arrests followed by the activation of the extrinsic and intrinsic apoptotic pathways, necroptosis and autophagic cell death.

3.6. KB2 triggers intrinsic and extrinsic apoptosis and necroptosis in breast cancer cells

When cells are unable to repair DNA damage, biochemical cascades are activated that lead to one or more forms of programmed cell death (PCD) such as apoptosis, autophagy (PCD type II) and programmed necrosis (PCD type III), also known as necroptosis. Light microscopy analyses revealed that KB2 induced characteristic features of apoptosis including chromatin condensation, cell shrinkage and membrane blebbing (Fig. 5A). Western blot analyses showed that the levels of cleaved caspase 9 and 8, the initiator caspases for intrinsic and extrinsic apoptosis respectively, increased in response to KB2 treatment (Fig. 5B). It would, however, appear that while the activation of caspase 9 is more robust at 24 h, this is true for caspase 8 activation at 48 h of KB2 treatment. This correlated with increased levels of the active (cleaved) forms of the executioner caspases 3/7 and their substrate poly (ADP-ribose) polymerase (PARP). Together these results indicated that while KB2 induced both apoptotic pathways in the breast cancer cells tested, it triggerered the intrinsic apoptotic pathway before the extrinsic apoptotic pathway. The ability of anti-cancer drugs to activate both intrinsic and extrinsic apoptosis is advantageous because many cancer cells are capable of overriding the intrinsic pathway which compromises their effectiveness (Rebucci and Michiels, 2013).

While most cancer cells initially respond to proapoptotic drugs, they frequently acquire the ability to bypass the apoptotic pathway and develop drug resistance leading to tumour recurrence (Ouyang et al., 2012; Su et al., 2016). It is therefore predicted that for sustainable activity anti-cancer drugs need to trigger multiple PCD pathways such as necroptosis and autophagy. Phosphorylated receptor-interacting serine/threonine protein kinase 3 (p-RIP3) and its substrate mixed lineage kinase domain-like protein (p-MLKL) are critical components of necroptosis with p-MLKL being a key executioner of the process. We showed using western blotting that the levels of p-RIP3 increased under all conditions of KB2 treatment in the breast cancer cells (Fig. 5B). However, while this correlated with an increase in p-MLKL in MDA-MB-231 cells at 24 h and 48 h of KB2 treatment, p-MLKL levels increased only in MCF-7 cells at 24 h of KB2 treatment.

3.7. KB2 induces autophagic cell death in breast cancer cells

When the MCF-7 and MDA-MB-231 breast cancer cells were treated with KB2 we observed what appeared to be autophagic vesicles (Fig. 6A). During autophagy, LC3I, the cytosolic form of the microtubule-associated protein light chain 3 (LC3), is conjugated by phosphatidylethanolamine to form LC3II which remains bound to the autophagosome membrane and it is widely used as a marker of autophagy. To confirm that KB2 does indeed induce autophagy in the breast cancer cells tested, we therefore performed immunocytochemistry and western blotting with an antibody to LC3. Results showed that KB2 induced a time-dependent increase in, what is presumed to be, LC3II staining (Fig. 6B) and LC3II levels (Fig. 6C). It is important to note that in the cancer context, autophagy may assist in meeting the energy demands of established tumour cells but has also been implicated in cell death (Hanahan and Weinberg, 2011; Su, Mei and Sinha, 2013). Indeed, the induction of autophagy by anti-cancer drugs has been shown to play either a pro-death or pro-survival role, depending on the context. For example, cisplatin induced autophagy was shown to play a pro-survival role in esophageal cancer cells (Liu et al., 2011). On the other hand, autophagy induced by the palladacycle AJ-5 was shown to play a pro-death role in melanoma and breast cancer cells (Aliwaini et al., 2013, 2015). Therefore to determine whether KB2 induced autophagy is a pro-death or pro-survival mechanism, we measured the impact of blocking autophagy with bafilomycin-A1 on the effect of KB2 on cell viability. The results showed that treatment of breast cancer cells with KB2 in the presence of bafilomycin-A1 led to an increase in 35% and 33% of MCF-7 and MDA-MB-231 cell viability respectively (Fig. 6D). These results confirmed that the autophagy induced by KB2 is a pro-cell death mechanism. It will be interesting to further investigate the effect of KB2-induced autophagy on KB2-induced apoptosis and necroptosis as well as the effect of activating autophagy alone, by for example LiCl treatment, on MCF-7 and MDA-MB-231 cell viability.

4. Conclusion

From these results we concluded that KB2 exhibits anti-cancer activity against ER+ and TN breast cancer cells by inducing oxidative stress and DNA double strand breaks which lead to cell cycle arrests and programmed cell death by extrinsic and intrinsic apoptotic pathways, necroptosis and autophagy (Fig. 7). The ability of KB2 to activate more than one mode of programmed cell death suggests that breast cancer cells are less likely to develop resistance to it. These results warrant further investigation of the anti-cancer activity and cytotoxicity of KB2 in an in vivo animal model.

Declaration of Competing Interest

The authors declare that they have no known competing financial interests or personal relationships that could have appeared to influence the work reported in this paper.

Acknowledgements

The authors were supported by grants from the South Africa Medical Research Council, the National Research Foundation (NRF) of South Africa, Cancer Association of South Africa (CANSA) and the University of Cape Town. The authors also acknowledge São Paulo State Foundation, Brazil, (FAPESP, grants # 2015/17177-6; 2018/08400-1; 2019/02008-5) for financial support.

References

Aliwaini, S., Swarts, A.J., Blanckenberg, A., Mapolie, S., Prince, S., 2013. A novel binuclear palladacycle complex inhibits melanoma growth in vitro and in vivo through apoptosis and autophagy. Biochem. Pharmacol. 86, 1650–1663. https://doi.org/10.1016/j.bcp.2013.09.020.

Aliwaini, S., Peres, J., Kröger, W.L., Blanckenberg, A., de la Mare, J., Edkins, A.L., Mapolie, S., Prince, S., 2015. The palladacycle, AJ-5, exhibits anti-tumour and anti-cancer stem cell activity in breast cancer cells. Cancer Lett. 357, 206–218. https://doi.org/10.1016/j.canlet.2014.11.027.

Bleloch, J.S., du Toit, A., Gibhard, L., Kimani, S., Ballim, R.D., Lee, M., Blanckenberg, A., Mapolie, S., Wiesner, L., Loos, B., Prince, S., 2019. The palladacycle complex AJ-5 induces apoptotic cell death while reducing autophagic flux in rhabdomyosarcoma cells. Cell Death Discov. 2019, 5. https://doi.org/10.1038/s41420-019-0139-9.

Bray, F., Ferlay, J., Soerjomataram, I., Siegel, R.L., Torre, L.A., Jemal, A., 2018. Global cancer statistics 2018: GLOBOCAN estimates of incidence and mortality worldwide for 36 cancers in 185 countries. CA. Cancer J. Clin. 68, 394–424. https://doi.org/10.3322/caac.21492.

Cappello, A.R., Aiello, F., Polerà, N., Armentano, B., Casaburi, I., Di Gioia, M.L., Loizzo, M.R., Dolce, V., Pezzi, V., Tundis, R., 2019. In vitro anti-proliferative and anti-bacterial properties of new C7 benzoate derivatives of pinocembrin. Nat. Prod. Res. 2019, 1–9. https://doi.org/10.1080/14786419.2019.1641805.

Chahar, M.K., Sharma, N., Dobhal, M.P., Joshi, Y.C., 2011. Flavonoids: a versatile source of anticancer drugs. Pharmacogn. Rev. 5, 1–12. https://doi.org/10.4103/0973-7847.79093.

Chen, H.M., Wu, Y.C., Chia, Y.C., Chang, F.R., Hsu, H.K., Hsieh, Y.C., Chen, C.C., Yuan, S. S., 2009. Gallic acid, a major component of *Toona sinensis* leaf extracts, contains a ROS-mediated anti-cancer activity in human prostate cancer cells. Cancer Lett. 286, 161–171. https://doi.org/10.1016/j.canlet.2009.05.040.

Chen, Z., Rasul, A., Zhao, C., Millimouno, F.M., Tsuji, I., Yamamura, T., Iqbal, R., Malhi, M., Li, X., Li, J., 2013. Antiproliferative and apoptotic efffects of pinocembrin in

human prostate cancer cells. Bangladesh J. Pharmacol. 8, 255–262. https://doi.org/10.3329/bjp.v8i3.14795.
Clifford, M.N., Toma, F.A., 2000. Flavanones, chalcones and dihydrochalcones – nature, occurrence and dietary burden. J. Sci. Food Agric. 1080, 1073–1080. https://doi.org/10.1080/14786419.2019.1641805.
Van De Beer, J.J.J., Wyk, B., 2011. An ethnobotanical survey of the Agter – Hantam, Northern Cape Province, South Africa. South African J. Bot. 77, 741–754. https://doi.org/10.1016/j.sajb.2011.03.013.
Dongre, A., Weinberg, R.A., 2019. New insights into the mechanisms of epithelial–mesenchymal transition and implications for cancer. Nat. Rev. Mol. Cell Biol. 20, 69–84. https://doi.org/10.1038/s41580-018-0080-4.
Eichsteininger, J., Kirisits, K., Smöch, C., Stadlbauer, C., Nguyen, C.H., Jäger, W., Özmen, A., Ecker, G., Krupitza, G., Krenn, L., 2019. Structural insight into the in vitro anti-intravasative properties of flavonoids. Sci. Pharm. 87. https://doi.org/10.3390/scipharm87030023.
Elbagory, A.M., Meyer, M., Cupido, C.N., Hussein, A.A., 2017. Inhibition of bacteria associated with wound Infection by biocompatible green synthesized gold nanoparticles from South African plant extracts. Nanomaterials 7, 1–22. https://doi.org/10.3390/nano7120417.
Fiebig, H.H., Maier, A., Burger, A.M., 2004. Clonogenic assay with established human tumour xenografts: correlation of in vitro to in vivo activity as a basis for anticancer drug discovery. Eur. J. Cancer. 40, 802–820. https://doi.org/10.1016/j.ejca.2004.01.009.
Hanahan, D., Weinberg, R.A., 2011. Review Hallmarks of Cancer : The Next Generation. Cell. Elsevier Inc. 144 (5), 646–674. https://doi.org/10.1016/j.cell.2011.02.013.
Johnson, D.G., Walker, C.L., 1999. Cyclins and cell cycle checkpoints. Annu. Rev. Pharmacol. Toxicol. 39, 295–312. https://doi.org/10.1146/annurev.pharmtox.39.1.295.
Keskes, H., Belhadj, S., Jlail, L., El Feki, A., Damak, M., Sayadi, S., Allouche, N., 2017. LC-MS-MS and GC-MS analyses of biologically active extracts and fractions from Tunisian *Juniperus phoenice* leaves. Pharm. Biol. 55, 88–95. https://doi.org/10.1080/13880209.2016.1230139.
Koch, A., Tamez, P., Pezzuto, J., Soejarto, D., 2005. Evaluation of plants used for antimalarial treatment by the Maasai of Kenya. J. Ethnopharmacol. 101, 95–99. https://doi.org/10.1016/j.jep.2005.03.011.
Kumar, M.A.S., Nair, M., Hema, P.S., Mohan, J., Santhoshkumar, T.R., 2007. Pinocembrin triggers Bax-dependent mitochondrial apoptosis in colon cancer cells. Mol. Carcinog. 241, 231–241. https://doi.org/10.1002/mc.
Liu, D., Yang, Y., Liu, Q., Wang, J., 2011. Inhibition of autophagy by 3-MA potentiates cisplatin-induced apoptosis in esophageal squamous cell carcinoma cells. Medical Oncology 28 (1), 105–111. https://doi.org/10.1007/s12032-009-9397-3.
Mativandlela, S.P.N., Meyer, J.J.M., Hussein, A.A., Houghton, P.J., Hamilton, C.J., Lall, N., 2008. Activity against *Mycobacterium smegmatis* and *M. tuberculosis* by extract of South African medicinal plants. Phyther. Res. 22, 841–845. https://doi.org/10.1002/ptr.2378.
Mativandlela, S.P.N., Muthivhi, T., Kikuchi, H., Oshima, Y., Hamilton, C., Hussein, A. A., Van Der Walt, M.L., Houghton, P.J., Lall, N., 2009. Antimycobacterial flavonoids from the leaf extract of *Galenia africana*. J. Nat. Prod. 72, 2169–2171. https://doi.org/10.1021/np800778b.
Navaneethakrishnan, S., Rosales, J.L., Lee, K., 2019. ROS-mediated cancer cell killing through dietary phytochemicals. Oxid. Med. Cell. Longev. 2019, 1–9. https://doi.org/10.1155/2019/9051542.
Ng'uni, T.L., 2017. Medicinal Uses of Galenia africana: A Study of the Antimicrobial, Antifungal and Anticancer Properties, (unpublished doctoral dissertation). University of Western Cape, Bellville, South Africa.
Ouyang, L., Shi, Z., Zhao, S., Wang, F.T., Zhou, T.T., Liu, B., Bao, J.K., 2012. Programmed cell death pathways in cancer: a review of apoptosis, autophagy and programmed necrosis. Cell Prolif. 45, 487–498. https://doi.org/10.1111/j.1365-2184.2012.00845.x.
Qian, C.N., Mei, Y., Zhang, J., 2017. Cancer metastasis: issues and challenges. Chin. J. Cancer 36, 36–39. https://doi.org/10.1186/s40880-017-0206-7.
Rasul, A., Millimouno, F.M., Eltayb, W.A., Ali, M., Li, J., Li, X., 2013. Pinocembrin : a novel natural compound with versatile pharmacological and biological activities. Biomed. Res. Int. 2013, 1–9. https://doi.org/10.1155/2013/379850.
Rebucci, M., Michiels, C., 2013. Molecular aspects of cancer cell resistance to chemotherapy. Biochem. Pharmacol. 85, 1219–1226. https://doi.org/10.1016/j.bcp.2013.02.017.
Russo, T., Zambrano, N., Esposito, F., Ammendola, R., Cimino, F., Fiscella, M., Jackman, J., O'Connor, P.M., Anderson, C.W., Appella, E., 1995. A p53-independent pathway for activation of WAF1/CIP1 expression following oxidative stress. J. Biol. Chem. 270, 29386–29391. https://doi.org/10.1074/jbc.270.49.29386.
Shaltiel, I.A., Krenning, L., Bruinsma, W., Medema, R.H., 2015. The same, only different – DNA damage checkpoints and their reversal throughout the cell cycle. J. Cell Sci. 128, 607–620. https://doi.org/10.1242/jcs.163766.
Srivastava, S., Somasagara, R.R., Hegde, M., 2016. Quercetin, a natural flavonoid interacts with DNA, arrests cell cycle and causes tumor regression by activating mitochondrial pathway of apoptosis. Sci. Rep. 2016, 1–13. https://doi.org/10.1038/srep24049.
Su, M., Mei, Y., Sinha, S., 2013. Role of the Crosstalk between Autophagy and Apoptosis in Cancer. J Oncol. 2013, 102735. https://doi.org/10.1155/2013/102735.
Su, Z., Yang, Z., Xie, L., Dewitt, J.P., Chen, Y., 2016. Cancer therapy in the necroptosis era. Cell Death Differ. 23, 748–756. https://doi.org/10.1038/cdd.2016.8.
Ticha, L.A., Klaasen, J., Green, I.R., Naidoo, G., 2015. Phytochemical and antimicrobial screening of flavanones and chalcones from *Galenia africana* and *Dicerothamnus rhinocerotis*. Nat. Prod. Commun. 10, 1185–1190. https://doi.org/10.1177/1934578x1501000713.
Tiloke, C., Phulukdaree, A., Chuturgoon, A.A., 2013. The antiproliferative effect of *Moringa oleifera* crude aqueous leaf extract on cancerous human alveolar epithelial cells. BMC Complement. Altern. Med. 13, 1–8. https://doi.org/10.1186/1472-6882-13-226.
Vallejo, M.J., Salazar, L., Grijalva, M., 2017. Oxidative stress modulation and ROS-mediated toxicity in cancer: a review on in vitro models for plant-derived compounds. Oxid. Med. Cell. Longev. 2017, 1–9. https://doi.org/10.1155/2017/4586068.
Van Wyk, B., De Wet, H., Van Heerden, F.R., 2008. An ethnobotanical survey of medicinal plants in the southeastern Karoo, South Africa. South African J. Bot. 74, 696–704. https://doi.org/10.1016/j.sajb.2008.05.001.
Vries, F.A., El Bitar, H., Green, I.R., Klaasen, J.A., Mabulesa, W.T., Bodo, B., Johnson, Q., 2005. An antifungal active extract from the aerial parts of *Galenia africana*. In: 11th NAPRECA Symposium Book of Proceedings. Antananarivo, Madagascar, pp. 123–131.
Yaacob, N.S., Kamal, N.N.N.M., Norazmi, M.N., 2014. Synergistic anticancer effects of a bioactive subfraction of *Strobilanthes crispus* and tamoxifen on MCF-7 and MDA-MB-231 human breast cancer cell lines. BMC Complement. Altern. Med. 14, 1–13. https://doi.org/10.1186/1472-6882-14-252.
Zhang, Z., Chen, S., Mei, H., Xuan, J., Guo, X., Couch, L., 2015. *Ginkgo biloba* leaf extract induces DNA damage by inhibiting topoisomerase II activity in human hepatic cells. Sci. Rep. 1–13. https://doi.org/10.1038/srep14633.